# Maneuver Detection and Estimation with Optical Tracklets

**Keric Hill**
*Pacific Defense Solutions (IAI), 535 Lipoa Pkwy, Suite 101, Kihei, HI 96753.*

## ABSTRACT

A method is proposed for detecting and estimating maneuvers using optical (angles-only) tracklets. After the correlator recognizes that a Resident Space Object (RSO) has maneuvered and no longer matches its pre-maneuver trajectory, observations for that RSO will be classified as Uncorrelated Tracks (UCTs). Using an algorithm to indicate when known RSOs have gone missing, an initial estimate for a maneuver can be obtained by processing the pool of UCTs with an algorithm called Two Angle Pairs Initial Orbit with Conjunction Analysis (TAPIOCA). TAPIOCA computes hypothesized orbits on the admissible region for two angles-only observations and back-propagates the orbits to look for conjunctions with the last known trajectories for the missing RSOs. If a conjunction is found with a small miss distance and velocity difference, it is used as an estimate for a maneuver. Once an initial estimate for the maneuver is obtained from TAPIOCA, a batch least-squares process is outlined which can refine that maneuver estimate and provide predictions for the trajectory and covariance after the maneuver such that the correlator will correctly identify that object for subsequent tracklets. As more tracklets become available after the maneuver, it is continually refined in the least-squares estimator. The maneuver estimates include start time and thrust. Maneuver detection results are shown for both simulated and real geostationary objects. Using Raven observations of Galaxy 15, the method was able to find five maneuvers over four weeks which were verified against precise WAAS ephemeris.

## 1. INTRODUCTION

When tracking non-cooperative Resident Space Objects (RSOs), detecting and estimating maneuvers can be difficult, especially when using optical (angles-only) observations. If a small maneuver is not detected, the orbit estimate and the orbit error covariance will be corrupted for a period of time. For large maneuvers, undetected maneuvers can lead to either the post-maneuver observations not correlating properly or the sensor not pointing close enough to the RSO to observe it, in which case the RSO will be lost.

For large maneuvers, determining which observations correspond to the post-maneuver RSO can be difficult if the post-maneuver orbit is not similar enough for the correlator to function reliably. When correlating the post-maneuver observations is not a problem, the maneuver is usually found using visual inspection. In order to use batch least-squares estimation, the orbit estimation process is usually re-started using only the observations after the maneuver[1]. The problem with angles-only data is that an accurate orbit estimate is not available until the RSO has been observed over several hours. In the mean time, there is not a good orbit estimate to use for pointing the sensor or correlating observations. Once the new post-maneuver orbit estimate is available, it can then be back-propagated to look for intersections between the pre-maneuver trajectory and the post-maneuver trajectory and computing a more exact maneuver time[2]. A sequential filter does not have to be re-started and a smoother can be used to estimate maneuver parameters, if *a priori* knowledge of the commanded maneuver is available through outside sources, or through the work of an analyst[3].

The method in this paper was designed to enable automated detection of both large and small maneuvers. The first step is maneuver detection, which is recognizing when an RSO has maneuvered. For small maneuvers, that usually happens when the residual RMS of the observations becomes large in a batch least-squares estimator. Larger maneuvers are detected when the post-maneuver observations of the RSO no longer correlate. After a maneuver causes an RSO to go unrecognized by the correlator, observations for that RSO become Uncorrelated Tracks (UCTs). Also, recently correlated observations which result in a high residual RMS in the orbit estimator are rejected and likewise tagged as UCTs. The next step is recognizing that an RSO has gone missing, i.e. knowing it should have been seen and correlated when it wasn't. Then an initial estimate for the maneuver is obtained by processing the pool of UCTs and comparing them to the last known trajectory for the missing RSO. Once an initial estimate for the maneuver is obtained with sufficient accuracy, the last step is to use a batch least-squares process to refine that maneuver estimate

(without restarting) and provide predictions for the trajectory and covariance after the maneuver such that the correlator will correctly identify that object for subsequent observations. Details of this process are described in the following sections.

## 2. TAPIOCA

With a single tracklet, defined as short set of optical observations of an RSO typically spanning less than a minute, it is impossible to determine an orbit due to the observability limitations of the angles-only data. An initial orbit "guesstimator" has been implemented called Two Angle Pairs Initial Orbit with Conjunction Analysis (TAPIOCA). This IOD technique was first designed to find an orbit estimate using a single tracklet which most closely matches a set of nominal orbital elements. TAPIOCA returns that orbit estimate along with a quality-of-fit metric, $\varepsilon$.

A tracklet cannot be used to uniquely determine an orbit because the observed motion of the satellite is nearly linear for the short time the satellite is observed. The two angle pairs of right ascension and declination at the beginning and end of the span provide on example of four independent measurements that can be extracted from the tracklet. In TAPIOCA, those two pairs of right ascension and declination ($\alpha_i$,$\delta_i$) angles are converted to line-of-sight (LOS) unit vectors ($\hat{\mathbf{o}}_\mathbf{i}$).

$$\hat{\mathbf{o}}_\mathbf{i} = \begin{bmatrix} \cos\delta_i \cos\alpha_i \\ \cos\delta_i \sin\alpha_i \\ \sin\delta_i \end{bmatrix} \tag{1}$$

Using the two LOS vectors ($\hat{\mathbf{o}}_\mathbf{1}$, $\hat{\mathbf{o}}_\mathbf{2}$), the two observer position vectors ($\mathbf{q_1}$, $\mathbf{q_2}$), and the corresponding times ($t_1$,$t_2$), the target's position, $\mathbf{r_i}$, and velocity, $\mathbf{v_i}$, are estimated.

The two unknowns needed to uniquely determine an orbit are the ranges at the tracklet end points, which can be represented by the range at the initial point, $\rho_1$, and the average range-rate over the streak, $\dot{\rho}$. For each combination of ranges, there exists a possible orbit solution. We are only interested in Earth-orbiting satellites, and only certain combinations of ranges will result in elliptical orbits. That region of elliptical orbits is called the "admissible region"[4].

In order to compute the orbital elements, the position and velocity of the spacecraft are needed. The positions are

$$\mathbf{r_1} = \rho_1 \hat{\mathbf{o}}_\mathbf{1} + \mathbf{q_1} \tag{2}$$

$$\mathbf{r_2} = (\rho_1 + \Delta\rho)\, \hat{\mathbf{o}}_\mathbf{2} + \mathbf{q_2}\,, \tag{3}$$

where

$$\Delta\rho = \dot{\rho}\,(t_2 - t_1)\ . \tag{4}$$

For a very short arc, it is assumed that the spacecraft accelerates very little, so the velocity at the start and stop times is the same and

$$\mathbf{v_1} = \mathbf{v_2} = \frac{\mathbf{r_2} - \mathbf{r_1}}{t_2 - t_1}\,. \tag{5}$$

For longer tracklets, the assumption that velocity is constant over the entire span is no longer adequate, so if the tracklet spans longer than 10 seconds, a Lambert solution is obtained using Gooding's Lambert solver[5] in order to find the velocity at each observation time.

The resulting values for $\mathbf{r_1}$ and $\mathbf{v_1}$ are used to compute the specific mechanical energy, $\xi$, of the orbit. If $\xi < 0$, the orbit is elliptical.

$$\xi = \frac{|\mathbf{v_1}|^2}{2} - \frac{\mu}{|\mathbf{r_1}|} \tag{6}$$

### 2.1 Optimization

The core of TAPIOCA is a hill-climbing optimization routine which finds an orbit within the admissible region that most closely matches a set of four orbital element targets. The targeted elements, which are not all independent, are semimajor axis, $a$, eccentricity, $e$, inclination $i$, and radius of perigee, $r_p$. There is an option to target radius of apogee, $r_a$, instead of $r_p$. Along with target values for each of the four elements

($x_a$, $x_e$, $x_i$, and $x_{rp}$ or $x_{ra}$), scale factors are also provided, ($S_a$, $S_e$, $S_i$, and $S_{rp}$ or $S_{ra}$). The larger the scale factor for a given element, the larger the error can be and still be acceptable. Using an initial guess for the range and range-rate ($\rho_1$ and $\dot{\rho}$), the optimization routine computes orbital elements and the error metric, $\varepsilon$.

$$\varepsilon = \left(\frac{a - x_a}{S_a}\right)^2 + \left(\frac{e - x_e}{S_e}\right)^2 + \left(\frac{i - x_i}{S_i}\right)^2 + \left(\frac{r_p - x_{rp}}{S_{rp}}\right)^2 . \tag{7}$$

Then a search is performed to minimize $\varepsilon$ using a steepest-descent Hill-climbing method with variable step size. That involves computing $\varepsilon$ in eight locations evenly spaced in a circle around the initial point. The point with the lowest metric which is lower than the current $\varepsilon$ is selected as the next central point and the process is repeated. If the algorithm moves in the same direction three times, the step sizes are doubled. If the algorithm does not find a lower value of $\varepsilon$ among the eight points, the step size is halved and the process is repeated until either the step size for $\Delta\rho$ is less than 0.01 km, $\varepsilon$ is less than 0.25, or the number of iterations is greater than 250. The three convergence criteria can be easily adjusted to tune the performance of the algorithm. A special mode is used to move along mathematically challenging "ridges and alleys."

### 2.2 Reduced Tracklets

Instead of iterating on the unknown ranges at the tracklet endpoints, a tracklet can be reduced to a single observation with angles and their rates with less noise. The LOS vector at the tracklet midpoint is $\hat{\mathbf{o}}_{mid}$, the observer position is $\mathbf{q}_{mid}$, and the observer velocity is $\dot{\mathbf{q}}_{mid}$. The range and range-rate at the midpoint are $\rho_{mid}$ and $\dot{\rho}_{mid}$. The position of the target at the tracklet midpoint, $\boldsymbol{r}_{mid}$, is

$$\boldsymbol{r}_{mid} = \rho_{mid}\,\hat{\mathbf{o}}_{mid} + \mathbf{q}_{mid}\,. \tag{8}$$

The velocity of the target at the tracklet midpoint becomes

$$\mathbf{v}_{mid} = \rho_{mid}\left[\tan(\dot{\alpha})\cos(\delta)\hat{\boldsymbol{\alpha}} + \tan(\dot{\delta})\hat{\boldsymbol{\delta}}\right] + \dot{\rho}_{mid}\,\hat{\mathbf{o}}_{mid} + \dot{\mathbf{q}}_{mid}\,, \tag{9}$$

where $\hat{\boldsymbol{\alpha}}$ and $\hat{\boldsymbol{\delta}}$ are unit vectors perpendicular to the line of sight pointing along the apparent right ascension and declination directions

$$\hat{\boldsymbol{\alpha}} = \frac{\begin{bmatrix} 0 & 0 & 1 \end{bmatrix}^T \times \hat{\mathbf{o}}_{mid}}{\left|\begin{bmatrix} 0 & 0 & 1 \end{bmatrix}^T \times \hat{\mathbf{o}}_{mid}\right|} \tag{10}$$

$$\hat{\boldsymbol{\delta}} = \hat{\mathbf{o}}_{mid} \times \hat{\boldsymbol{\alpha}}\,. \tag{11}$$

When more accuracy is desired, instead of iterating on $\rho_1$ and $\dot{\rho}$, the optimization process iterates on $\rho_{mid}$ and $\dot{\rho}_{mid}$.

## 3. MANEUVER DETECTION

TAPIOCA has an option to perform a conjunction analysis instead of finding orbits close to a nominal set of elements. To do that, the optimization routine finds an orbit that passes close to the trajectory of another satellite in the future. The result is a conjunction time, miss distance ($\Delta r$), and velocity difference ($\Delta v$). In the optimization routine, the targeted elements are $\Delta r$ and $\Delta v$ instead of nominal orbital elements. The target values for each of the two elements ($x_{\Delta v}$ and $x_{\Delta r}$) are usually set to zero, assuming that smaller maneuvers are more likely in order to conserve fuel[6]. The scale factors are $S_{\Delta v} = 10$ m/s, and $S_{\Delta r} = 10$ km. For conjunction analysis, TAPIOCA's IOD tool is first used to obtain an initial guess for the range and range rate ($\rho_1$ and $\dot{\rho}$), then the optimization routine computes orbital elements and a state vector. The state vector is propagated over a limited time period using a two-body propagator. Once the closest conjunction is found, the error metric, $\varepsilon$ is computed.

$$\varepsilon = \left(\frac{\Delta v}{S_{\Delta v}}\right)^2 + \left(\frac{\Delta r}{S_{\Delta r}}\right)^2 \tag{12}$$

This same technique can be used to find possible conjunctions in the future, or possible maneuvers in the past, since both are simply the intersections of two trajectories. For conjunction analysis or maneuver detection, extra accuracy is needed, so TAPIOCA uses reduced tracklets and applies a light-time correction where the time of the estimated state vector is adjusted back by the light travel time computed from the latest range estimate. In addition, when close to finding a final solution, the hypothesized orbit state is propagated using an SP orbit propagator instead of the default two-body propagator.

TAPIOCA's conjunction analysis tool was used with a single tracklet which occurred 17 minutes after a maneuver of 2.5 m/s. A portion of the admissible region for this example is shown in Figure 1. The colored contours represent miss distance (with the color scale shown on the right in km) and the dashed magenta lines show contours for the $\Delta$v in m/s. The course taken by the hill-climbing method is shown with red dots connected by lines, which in this case are all bunched together. While the final estimate of range and range-rate (red square) were close to the truth (white star), the conjunction found was 16 minutes after the maneuver (1 minute before the tracklet itself) and the $\Delta v$ was 49 m/s, neither of which are accurate. The computed miss distance was 2.5 km. In the map of the admissible region, there should be a point with both small miss distance (dark blue in the color coded contours) and small $\Delta v$, but there is not.

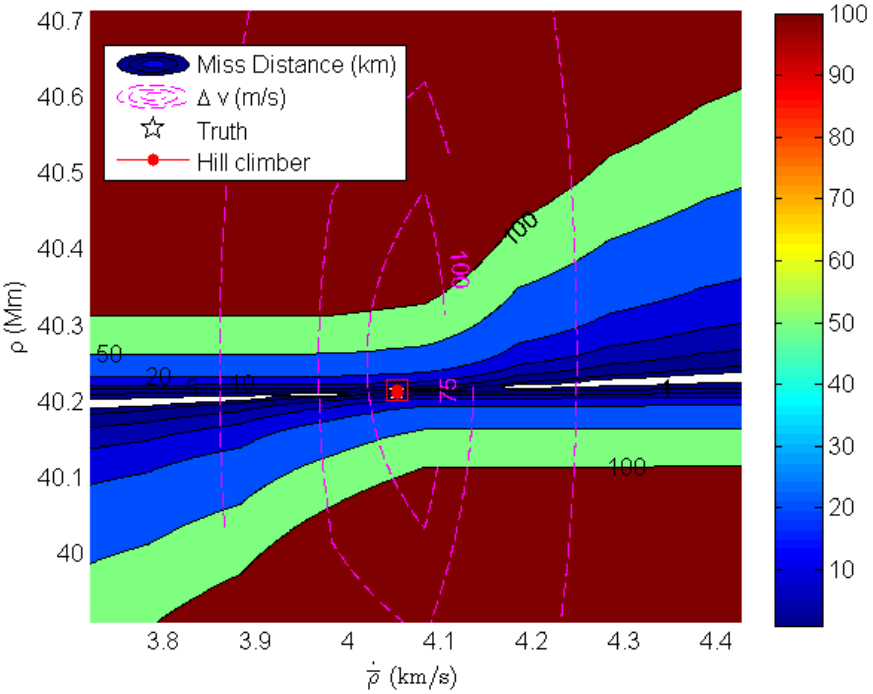


Figure 1: Maneuver Detection Contours for a Single Reduced UCT Tracklet.

### 3.1 Two-Tracklet Maneuver Detection

The problem with single-tracklet maneuver detection is that the angle rates are not known to sufficient accuracy and thus the hypothesized trajectories are not close enough to the truth to give valid results. TAPIOCA can operate using two observations separated by longer time spans using Gooding's Lambert solver. In this case, two reduced tracklets are used for the observations in the same way that tracklet endpoints were used earlier. A second tracklet taken three minutes after the first was used in TAPIOCA with the results shown in Figure 2.

The conjunction found was 4 minutes after the true maneuver and the $\Delta v$ was 2.2 m/s, which is much closer to the actual maneuver. It appears that at least several minutes of arc are required to get valid angle rates and find a maneuver using the TAPIOCA algorithm.

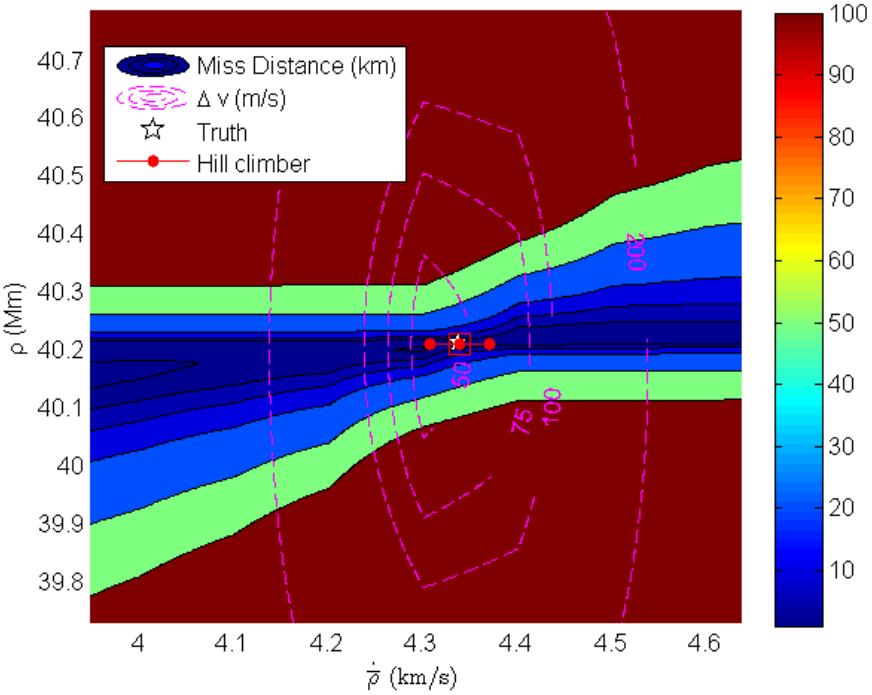


Figure 2: Admissible Region for Two UCT Tracklet Fits.

## 4. MANEUVER ESTIMATION

Maneuvers are modeled using a thrust vector in Newtons, $\mathbf{F}_{man}$, a coordinate system for the thrust vector, a start time, $t_{man,i}$, a stop time $t_{man,f}$, and a specific impulse, $I_{sp}$. The acceleration due to a maneuver is

$$\ddot{\mathbf{r}}_{man} = \left[\frac{\partial INERTIAL}{\partial MAN}\right]_{3\times 3} \frac{\mathbf{F}_{man}}{m_{sat}} \frac{1\,\mathrm{km}}{1000\,\mathrm{m}}\,, \tag{13}$$

where $\left[\frac{\partial INERTIAL}{\partial MAN}\right]$ is the rotation from the maneuver coordinate system to the inertial coordinate system used for the orbit. The radial, along-track, and cross-track coordinate system was always used for maneuvers in this study. The value $m_{sat}$ is the mass of the spacecraft in kg. When position and velocity are defined in units of km and km/s, a conversion is required to change the acceleration to units of km/s$^2$. In order for the propagation to be accurate, the propagation time step must stop exactly at $t_{man,i}$ and $t_{man,f}$.

Once an initial maneuver estimate is obtained, it is refined in a batch least-squares estimator. In this case, The spacecraft state, $\mathbf{X}$, consists of three position and velocity components, the reflectance, $c_R$, the maneuver thrust vector, $\mathbf{F}_{man}$, and the maneuver start time, $t_{man,i}$. The maneuver is assumed to have a short duration of 1 millisecond, so it is nearly impulsive.

$$\mathbf{X} = [\ x \quad y \quad z \quad \dot{x} \quad \dot{y} \quad \dot{z} \quad c_R \quad \mathbf{F}_{man} \quad t_{man,i}\ ]^T\,. \tag{14}$$

The equations of motion are written

$$\dot{\mathbf{X}} = F(\mathbf{X}, t)\,. \tag{15}$$

An observation at time $t_i$ is denoted by $\mathbf{Y}_i$, and the state deviation and observation residuals are written

$$\mathbf{x}(t) = \mathbf{X}(t) - \mathbf{X}^*(t), \qquad \mathbf{y}(t) = \mathbf{Y}(t) - \mathbf{Y}^*(t), \tag{16}$$

where $\mathbf{X}^*$ is the reference solution, or the "best guess" orbit, and $\mathbf{Y}^*$ is an observation computed using the reference solution[7]. The observations can be related to the state with the $\tilde{H}$ matrix, which is

$$\tilde{H}_i = \left[\frac{\partial G}{\partial \mathbf{X}}\right]^*_i. \tag{17}$$

$G$ is a function that computes observations from a state vector

$$\mathbf{Y}_i = G(\mathbf{X}_i, t_i) + \epsilon_i \,. \tag{18}$$

$\epsilon_i$ is the observation error. State deviations at time $t$ are mapped back to the epoch, $t_k$, with the state transition matrix $\Phi$:

$$\mathbf{x}(t) = \Phi(t, t_k)\mathbf{x}(t_k). \tag{19}$$

The state transition matrix is integrated along with the state using the following relation:

$$\dot{\Phi}(t, t_k) = A(t)\Phi(t, t_k) \qquad \text{where} \qquad A(t) = \frac{\partial F(\mathbf{X}^*, t)}{\partial \mathbf{X}(t)} \,. \tag{20}$$

Relating an observation at time $t_i$ back to the state initial epoch $t_k$ is done with the $H_i$ matrix:

$$H_i = \tilde{H}_i \Phi(t_i, t_k) \tag{21}$$

So $H_i$ is the observation-state relationship at $t_i$ mapped back to the initial epoch $t_k$. A least squares solution for $\mathbf{x}(t_k)$ is computed with the equation

$$\hat{\mathbf{x}} = (H^T W H)^{-1} H^T W \mathbf{y} \,, \tag{22}$$

where $H$ includes all the $H_i$ matrices and $W$ is a weighting matrix and is the inverse of the measurement noise covariance.

To estimate the force vector $\mathbf{F}_{man}$, a portion of the $A$ matrix will contain the partials

$$\frac{\partial \ddot{\mathbf{r}}_{man}}{\partial \mathbf{F}_{man}} = \left[\frac{\partial INERTIAL}{\partial MAN}\right]_{3\times 3} \frac{1}{m_{sat}} \frac{1\,\text{km}}{1000\,\text{m}} \tag{23}$$

There is an option to estimate corrections to the maneuver start time or burn duration, with both parameters in seconds. However, it will usually be impossible to estimate both the complete force vector and the duration together, so in all the analysis presented, the duration will be fixed and the force vector estimated.

When estimating the start time, $t_{man,i}$, the standard deviation of the error in $t_{man,i}$ is $\sigma_{t,man,i}$. There are additional stop conditions in the propagation starting at $t_{man,i} - 3\sigma_{t,man,i}$ and $t_{man,f} + 3\sigma_{t,man,i}$. The partials at time $t$ with respect to the start time used in the variational equations are

$$\frac{\partial \ddot{\mathbf{r}}_{man}}{\partial t_{man,i}} = \left[\mathcal{N}(t \mid t_{man,f},\, \sigma^2_{t,man,i}) - \mathcal{N}(t \mid t_{man,i},\, \sigma^2_{t,man,i})\right] \ddot{\mathbf{r}}_{\mathbf{man}} \,, \tag{24}$$

where $\mathcal{N}(t \mid t_{man,i},\, \sigma^2_{t,man,i})$ is the probability density function at time $t$ with mean $t_{man,i}$ and variance $\sigma^2_{t,man,i}$.

$$\mathcal{N}(t \mid t_{man,i},\, \sigma^2_{t,man,i}) = \frac{1}{\sqrt{2\pi\sigma^2_{t,man,i}}}\, e^{\left[-\dfrac{(t - t_{man,i})^2}{2\sigma^2_{t,man,i}}\right]} \tag{25}$$

Since the acceleration due to the maneuver is not continuous in time, an infinitely small change in the start time will only affect the acceleration at the start and stop of the burn. The probability that the burn is starting at time $t$ is $\mathcal{N}(t \mid t_{man,i},\, \sigma^2_{t,man,i})$. At the start of the burn, a negative change in the start time leads to a positive increase in thrust, which is the reason for the negative sign on the term $\mathcal{N}(t \mid t_{man,i},\, \sigma^2_{t,man,i})$. The probability that the burn is ending at time $t$ is $\mathcal{N}(t \mid t_{man,f},\, \sigma^2_{t,man,i})$. At the end of the burn, a positive change in the start time leads to a positive increase in thrust, which is the reason for the positive sign on the term $\mathcal{N}(t \mid t_{man,f},\, \sigma^2_{t,man,i})$.

These partials are computed until the propagator reaches the stop condition at $t_{man,f} + 3\sigma_{t,man,i}$. It should be noted that the maneuver estimation process is highly non-linear and usually requires more iterations than typical batch least-squares. After a maneuver is detected, the maneuver estimation process is initiated. If the residual RMS from this maneuver estimation process is high, that maneuver hypothesis is rejected.

## 5. SIMULATION RESULTS

A simulation was performed using the TASMAN simulation architecture[8] to evaluate the performance of the maneuver detection and estimation. The simulation spanned 14 days from 1 January 2010 to 15 January 2010. In this simulation, the dynamical model included luni-solar gravity using JPL DE421 ephemerides[9], a 21×21 EGM2008 Earth gravity field[10], and a NRL MSIS atmospheric density model[11]. Solar radiation pressure (SRP) was set to 1367.0 W/m$^2$ at 1 AU. The simulations included a small telescope similar to a Raven located on Maui, and a simulated population of 1000 spherical RSOs in deep space orbits taken from a simulated debris catalog obtained in 2007 from Eugene Stansbury at NASA Johnson Space Center. There were also 24 catalog RSOs modeled as box-wing satellites with articulated solar arrays. Figure 3 shows the placement of the catalog RSOs. The satellites with an ID number greater than 9700 perform periodic station-keeping maneuvers in order to remain in a Geostationary Orbit (GEO) slot of ±0.05 degrees.

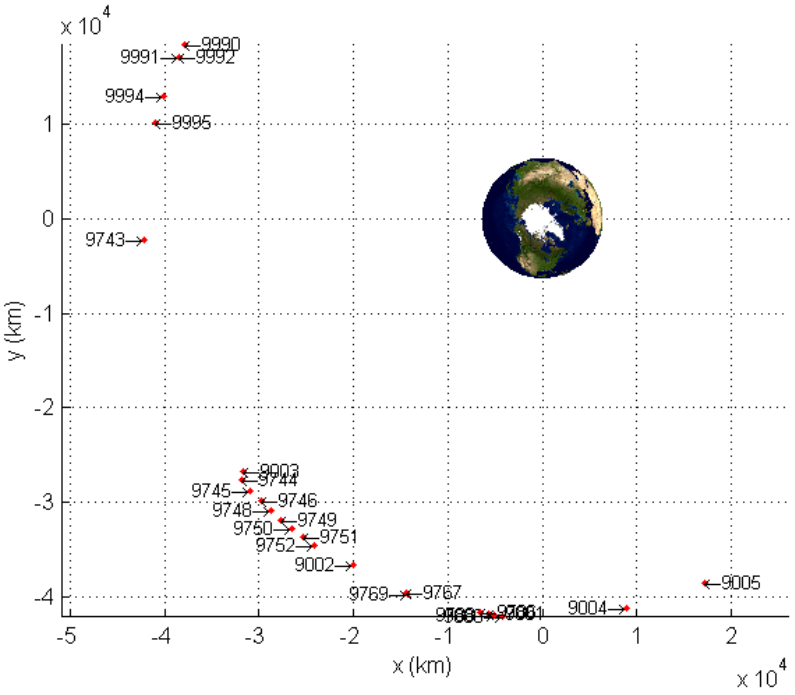


Figure 3: Simulated Catalog Satellites

To create an initial catalog, a seven-day precursor simulation with a perfect correlator but without maneuvers was used for only the catalog RSOs. For the catalog estimates, the satellites were (erroneously) modeled as diffuse spheres. The 1000 debris objects were not included in the catalog so that they would always show up as UCTs to potentially confuse the maneuver detection algorithm. Two of the 24 catalog RSOs, 9004 and 9005, turned out to not be visible from Maui, leaving 22 visible RSOs in the catalog. The sensor was scheduled to look at all visible catalog RSOs in turn, repeatedly from 5:00 to 15:00 UTC. Each sweep through all of the satellites took about 18 minutes. The sensor was pointed at the expected position of the satellite, which did not match the true position due to estimation errors. Observations were generated for any RSOs, including debris, in the FOV which were bright enough. All observations included light-time correction. Least-squares fits for the catalog estimates spanned seven days. Simulation time advanced in time steps of 15 minutes.

The maneuvers were detected and automatically applied to the catalog estimates for RSOs and continually updated in the estimation process as more observations were obtained and correlated to that RSO after the maneuver. For each UCT, maneuver hypotheses were generated for all the missing objects. This process was improved by first doing a feasibility check for each pair of UCTs formed. The feasibility check first verified that an elliptical orbit could be found with the proper range hypotheses. Next, a second feasibility

check verified that a Lambert solution connecting the two tracklets existed with angular rates that matched the observed rates. Then the conjunction analysis was performed to find if an orbit could be created from the two tracklets which could be back-propagated to intercept the pre-maneuver orbit. The thresholds for maximum acceptable maneuver miss distance and $\Delta$V were set to 10 km and 5 m/s, respectively.

Table 1: Maneuver Estimation Results from Simulation

| RSO | Time | Type | Start error (min) | $\Delta$V error (cm/s) | Detected |
|---|---|---|---|---|---|
| 9743 | 1 Jan 19:08 | E-W | 6.2 | 0.16 | 2 Jan 6:30 |
| 9995 | 1 Jan 20:40 | E-W | 40.4 | 0.50 | 2 Jan 7:30 |
| 9748 | 1 Jan 17:16 | N-S | 0.10[a] | 0.21[b] | 2 Jan 5:45 |
| 9788 | 2 Jan 17:13 | N-S | 0.21[a] | 0.22[b] | 3 Jan 5:45 |
| 9786 | 3 Jan 17:21 | N-S | 0.15[a] | 0.12[b] | 4 Jan 5:45 |
| 9748 | 5 Jan 8:56 | E-W | 9.96 | 0.18 | 6 Jan 5:15 |
| 9752 | 5 Jan 7:10 | E-W | 11.7 | 0.06 | 5 Jan 13:30 |
| 9749 | 5 Jan 17:14 | E-W | 21.7 | 0.30 | 6 Jan 5:30 |
| 9745 | 5 Jan 18:16 | E-W | 1.21 | 0.16 | 6 Jan 5:15 |
| 9749 | 6 Jan 8:13 | E-W | 2.55 | 0.25 | 7 Jan 5:30 |
| 9769 | 6 Jan 16:16 | N-S | 0.03[a] | 0.15[b] | 7 Jan 5:30 |
| 9991 | 8 Jan 0:25 | N-S | 572 | 4.54[b] | 8 Jan 8:30 |
| 9994 | 7 Jan 23:46 | E-W | 5.81 | 0.13 | 8 Jan 8:15 |
| 9992 | 8 Jan 0:25 | N-S | 0.10 | 0.30 | 8 Jan 8:30 |
| 9786 | 8 Jan 2:49 | E-W | 22.2 | 0.19 | 8 Jan 9:00 |
| 9991 | 8 Jan 0:25 | N-S | 438[c] | 86.3 | 8 Jan 9:00 |
| 9995 | 8 Jan 21:18 | N-S | 0.22 | 0.25 | 9 Jan 7:45 |
| 9990 | 9 Jan 0:31 | N-S | 0.10 | 0.22 | 9 Jan 8:30 |
| 9744 | 9 Jan 17:11 | E-W | 1.46 | 0.14 | 10 Jan 5:15 |
| 9769 | 9 Jan 15:45 | E-W | 2.33 | 0.12 | 10 Jan 5:30 |
| 9752 | 9 Jan 19:06 | N-S | 0.08 | 0.14 | 10 Jan 5:30 |
| 9992 | 9 Jan 10:08 | E-W | 3.12 | 0.11 | 10 Jan 8:15 |

[a] After correcting for ambiguous node crossing
[b] Direction reversed due to ambiguous node crossing
[c] Seems to correct for previous bad maneuver estimate

Since this simulation involved multiple maneuvering RSOs, sometimes in close proximity, in many cases there are multiple maneuver hypotheses. That is because sometimes there are multiple correct maneuver hypotheses using different pair-wise combinations of UCTs, and sometimes there are false maneuver hypotheses. The maneuver hypothesis with the lowest maneuver $\Delta$V, is taken as the most likely[6]. Later, if there are any other maneuver hypotheses for that same lost RSO, the UCT tracks are added to the observations tagged to that lost RSO but no additional (redundant) maneuver is applied. The rule is that no additional maneuvers are added to a catalog RSO estimate unless they are at least six hours apart. After a maneuver is applied to a catalog RSO estimate, that RSO is removed from the missing list.

Table 1 shows the results of maneuver estimation for 22 of the maneuvers. An additional 11 maneuvers were detected but had only preliminary estimates by the end of the simulation. In the table, the type of the maneuver indicates whether it was a North-South (N-S) or East-West (E-W) maneuver. N-S maneuvers occur at the node crossing when the RSO is either ascending or descending through the equatorial plane. Estimates for those maneuvers often place the maneuver during a different node crossing if more than one has occurred since the RSO was last seen. The time the maneuver was detected is specified in the simulation time to indicate how long it took for the maneuver to be found.

E-W maneuvers are so small, usually just a few cm/s, that they are hard to detect quickly. It usually takes many hours before they become apparent. On the other hand, N-S maneuvers are large enough to be detected quickly, however all of them occurred during daylight hours and could only be discovered at the beginning of the next night.

In general, the maneuver estimates are good to less than 1 cm/s. For E-W maneuvers, the error in the maneuver time was usually on the order of 10 minutes, while for N-S maneuvers, the maneuver time was correct to less than a minute (after shifting the maneuver time estimate by half periods until it was at the correct node crossing). The one bad result was for RSO 9991 on 8 January when it got the N-S $\Delta$V magnitude worse than usual ($\approx$2% error) and got the maneuver time off by several hours. After 30 minutes of simulation time, a second maneuver estimate was automatically applied to try and fix the problem. While neither maneuver seems very close to the actual maneuver, the combination somehow produced a good enough orbit for observations from 9991 to continue to correlate and update for the rest of the simulation.

## 6. REAL DATA RESULTS

To test maneuver detection using real data, observations of Galaxy 15 taken by a Raven-class telescope in Kihei, Maui were used from the following dates: May 15-18, May 21-25, May 29-June 1, and June 4-7 in 2013. Table 2 shows the maneuvers estimated. The "Trigger" is the process which first detected the maneuver, either the residual RMS or the correlator. Note that the estimated N-S maneuver times can be off by multiple half-revolutions for these particular cases since there were multiple node crossings during the observing gaps. The observing period extended from approximately 6:00 to 15:00 UTC, but Galaxy 15 usually became too dim to be detected sometime around 14:00 UTC. Most of the maneuvers occurred during the day, and they were not detected until the beginning of the next observing period.

Table 2: Maneuver Estimation Results for Galaxy 15

| Time | $\Delta$V (cm/s) | Type | Trigger | Detected |
|---|---|---|---|---|
| 17 May 14:20 | 2.2 | E-W | RMS | 18 May 6:12 |
| 20 May 22:30[a] | 154 | N-S | Correlator | 21 May 6:12 |
| 22 May 22:44 | 4.4 | E-W | Correlator | 23 May 6:06 |
| 30 May 22:33 | 8.7 | E-W | RMS | 31 May 13:00 |
| 3 Jun 21:19[a] | 150 | N-S | Correlator | 4 Jun 6:24 |

[a] The node crossing is ambiguous for this maneuver

Table 3: Maneuvers for Galaxy 15 Computed from WAAS Ephemeris

| Time | duration (sec) | $\Delta$V (cm/s) |
|---|---|---|
| 17 May 14:09:52 | 31.322 | 2.202 |
| 20 May 22:11:04 | 2241.668 | 154.62 |
| 22 May 22:42:21 | 64.262 | 4.369 |
| 30 May 14:50:40 | 43.034 | 3.010 |
| 3 Jun 21:16:13 | 2250.060 | 155.20 |

WAAS ephemerides for Galaxy 15 were obtained for the observation period and used for finding the true maneuver times. First, the position vectors from the ephemeris were used as observations in an Extended Kalman Filter (EKF). Position vectors which resulted in high residual errors indicated a deviation from the expected trajectory. Those times were used to divide the ephemeris into subsections. The discontinuity in velocity between the subsections was taken as an initial estimate of a maneuver. This was refined using least squares. To find the maneuver durations, the fit was run multiple times with different mass and levels of thrust. A good combination seemed to be a 1 N thruster and a spacecraft mass of about 1450 kg. Table 3 shows the maneuver information resulting from the analysis of the WAAS ephemeris. The estimated maneuver magnitudes for Galaxy 15 agree to within a few percent of those extracted from the WAAS ephemeris, with the exception of the one on May 30. That could be because very few observations were obtained the next four days after that maneuver. The first three estimated maneuver times were within a few minutes of the measured burn midpoints. The May 30 estimated maneuver time was off by about 8 hours. The June 3 N-S maneuver was off by about 16 minutes. The June 3 maneuver estimate also could

have been degraded by a lack of observations for the three days leading up to it. The times of the two N-S maneuvers were at the correct equatorial crossings, probably through luck more than anything else.

## 7. CONCLUSION

This method for automatically detecting and estimating both large and small maneuvers has been shown to be effective both in a simulation with a large number of maneuvering objects and using real data for a single satellite. This maneuver detection process is automated, which will free up human analysts for other tasks by substantially reducing the number of maneuvers that must be processed manually. This process also allows the post-maneuver trajectory to be recovered much more quickly than would be required to completely re-establish the trajectory and immediately provides post-maneuver covariance usable for further correlation. North-South station-keeping maneuvers could theoretically be detected within minutes while smaller East-West maneuvers usually required several hours. For this method to work, there must be at least two tracklets of the post-maneuver target separated by several minutes of time. While the estimated maneuvers were modeled as nearly impulsive, the software does allow for the estimation of longer duration, low-thrust burns.

## 8. ACKNOWLEDGEMENTS

This work was funded by the Air Force Research Laboratory under contract FA9451-13-C-0281.

## References

[1] Hirsch, B. J., *Maneuver Estimation Model for Geostationary Orbit Determination*, Master's thesis, Air Force Institute of Technology, June 2006.

[2] Kelecy, T. and Jah, M., "Detection and Orbit Determination of a Satellite Executing Low Thrust Maneuvers," *Acta Astronautica*, Vol. 66, No. 5-6, 2010, pp. 798–809.

[3] Hujsak, R. S., "Orbit Determination During High Thrust and Low Thrust Maneuvers," 2005, AAS 05-136, AAS/AIAA Space Flight Mechanics Conference, Copper Mountain, CO, Jan. 23-27.

[4] Milani, A., "The Asteroid Identification Problem. I. Recovery of Lost Asteroids," *Icarus*, Vol. 137, No. 2, 1999, pp. 269–292.

[5] Gooding, R., "A Procedure for the Solution of Lambert's Orbital Boundary-Value Problem," *Celestial Mechanics and Dynamical Astronomy*, Vol. 48, 1990, pp. 145–165.

[6] Holzinger, M. J., Scheeres, D. J., and Alfriend, K. T., "Object Correlation, Maneuver Detection, and Characterization Using Control-Distance Metrics," *Journal of Guidance, Control, and Dynamics*, Vol. 35, No. 4, 2012, pp. 1312–1325.

[7] Tapley, B. D., Schutz, B. E., and Born, G. H., *Statistical Orbit Determination*, Elsevier Academic Press, Burlington, MA, 2004.

[8] Hill, K., Sydney, P., Cortez, R., Hamada, K., , Nishimoto, D., Luu, K., and Schumacher, P. W., "Dynamic Tasking of Networked Sensors Using Covariance Information," 2010 AMOS Technologies Conference, Maui, HI, 14-17 Sep. 2010.

[9] Folkner, W. M., Williams, J. G., and Boggs, D. H., "JPL Planetary and Lunar Ephemeris, DE421," 2008, Jet Propulsion Laboratory Interoffice Memorandum IOM 343R-08-003, Mar. 31.

[10] Pavlis, N. K., Holmes, S., Kenyon, S., and Factor, J., "An Earth Gravitational Model to Degree 2160: EGM2008," 2008, General Assembly of the European Geosciences Union, Vienna, Austria, April 13-18.

[11] Picone, J., Hedin, A. E., Drob, D. P., and Aikin, A. C., "NRLMSISE-00 empirical model of the atmosphere: Statistical comparisons and scientific issues," *Journal of Geophysical Research*, Vol. 107, No. A12, 2002, pp. 1468.